CH_4-O_2 flame acceleration morphology: A comparative analysis under different hydrocarbon fuel, channel geometry and scale

Cristian C. Mejía-Botero, Florent Virot & Josué Melguizo-Gavilanes

Institute Pprime, UPR 3346 CNRS, ISAE-ENSMA, 86961, Futuroscope-Chasseneuil, France

1 Introduction

Under certain conditions, after accidental ignition of a flame, the latter may accelerate and transit to detonation, typically after interaction with obstacles, the so-called, deflagration-to-detonation-transition (DDT) scenarios. Detonation is a supersonic combustion propagation regime that is much stronger and more destructive than a flame. Although much less studied, in practice, DDT can also occur in narrow unobstructed spaces, such as fuel cells, battery packs, small scale electrolyzers, among others. The first stage of DDT is flame acceleration (FA) [1]; it is thus crucial to study it in an effort to further contribute to the understanding of this phenomenon.

Numerical simulations play an important role in the qualitative analysis of DDT [2]. Due to the high computational demands required to simulate DDT from first principles, simplifying assumptions are understandably made, i.e., axisymmetry. However, the latter assumptions have oftentimes not been verified by experimental evidence; this may be one of the reasons numerical simulations of DDT are not, as of yet, of predictive nature. In this work, a fully optically accessible polycarbonate channel, 1-m long with a square cross-section (10 mm $\times$ 10 mm) is used to characterize stoichiometric CH_4-O_2 FA via simultaneous schlieren visualization (SSV); the three-dimensional (3-D) flame morphologies that develop in the FA process can be thus unveiled. SSV was first demonstrated by Ballossier [3].

The morphologies are compared with those obtained by Krivosheyev et al. [4] in a 6-m long cylindrical tube with an inner diameter of 60 mm using an Argon diluted stoichiometric C_2H_2-O_2 mixture. This comparison is of interest since significant similarities were found in scenarios with a different hydrocarbon fuel, channel scale and cross section. Furthermore, it allows us to show the importance of characterizing the FA process via SSV since asymmetries are observed throughout.

2 Experimental methodology

The methodology proposed in [3, 5] is used in the current work. The channel has a square cross section of 10 x 10 mm^2 and 1 m length. To characterize the FA process in 3-D, the channel has full optical access with four polycarbonate windows, which are enclosed by an aluminum frame at the top and bottom to avoid bending as a result of the pressure attained during FA. The mixture is ignited by an electric

Correspondence to: cristian-camilo.mejia-botero@ensma.fr

arc located 3 mm from the closed end to minimize the dead volume and its influence on flame propagation [6]. The arc has an estimated electrical energy of less than 1 mJ to avoid direct detonation initiation. To perform a test, the following procedure is followed: (i) vacuum is applied to the channel until reaches a minimum pressure of 10 mbar, controlled by an MKS 220DA pressure sensor, (ii) a plastic cap closes the open end to keep the reactive mixture inside the channel, (iii) the premixed mixture is fed into the channel until it reaches atmospheric pressure, (iv) ignition is achieved by an electric arc; simultaneously the plastic cap is opened, (v) the optical configuration is triggered by the chemiluminescence captured by a photodiode. The channel is filled with a mixture composed of high purity O_2 ($99.9997\ \%$) and CH_4 ($99.95\ \%$) under stoichiometry conditions.

Two independent schlieren set-ups capture the side and bottom view of the channel. The cameras used for the side- and bottom-view, respectively, are: (i) a Shimadzu HPV-2, with a minimum frame rate of $125,000$ FPS (1000 ns exposure time) and a maximum of $1,000,000$ FPS (250 ns exposure time), and (ii) a Shimadzu HPV-X2 with a minimum frame rate of $200,000$ FPS (200 ns exposure time) and maximum $10,000,000$ FPS (50 ns exposure time). During the entire experimental campaign the FPS was fixed at $1,000,000$ for both cameras with exposure times of 200 ns and 250 ns for the HPV-X2 and HPV-2, respectively.

3 Results

3.1 Morphologies during FA

Figure 1 (a) shows the two-directional schlieren images captured during the FA process of the CH_4/O_2 mixture. The side and bottom view correspond to the position of the respective camera used. The images were recorded from $x = 50$ mm to $x = 450$ mm, being x the axial position in the channel. The run-up distance to DDT ($\bar{x}_{\text{DDT}}$) was $\bar{x}_{\text{DDT}} = 454$ mm so the results of FA just before the DDT are presented. The reference time ($t_{ref} = 0\ \mu$s) is taken at $x = 50$ mm. Figure 1 (b) presents the results obtained by Krivosheyev et al. [4]. High-speed flame front photography for a $25\ \%$ Argon-diluted stoichiometric C_2H_2/O_2 mixture during FA was performed. The experiments were carried out in a transparent cylindrical tube with an inner diameter of 60 mm and 6 m length (L). CH^* chemiluminescence was captured using Edmund Optics narrow-band optical filters (BP 430 ± 10 nm), coupled with two identical high-speed cameras Photron Fastcam SA-Z placed in parallel. Using these images it is possible to track the reactive flame front and its changes in morphology. The initial pressure of the test was 16 kPa. Note that the L/D_h ratio for both experiments is the same ($L/D_h = 100$) but the boundary conditions change since the tests performed by [4] were carried out in a channel closed on both ends. However, the large L/D_h ratio ensures that effects related to compression waves reflecting from the far end of the channel and their possible interaction with the front flame are avoided. For the stoichiometric CH_4/O_2 mixture, the sound speed in fresh gases is 373.4 m/s, taking 2.67 ms for a pressure wave to travel from the closed end to the open end of the channel. This time is longer than that required for the flame to reach $\bar{x}_{\text{DDT}}$ which precludes potential reflection wave-flame interactions.

When comparing the results in [4] with those obtained in the present work, very similar behaviors in the flame morphology during FA are observed. The finger-shape captured at $t = t_{ref} + 63\ \mu$s with the two-directional schlieren corresponds to the same morphology captured in the images $2 - 4$ by [4]. The flame in the image 1 is a hemi-sphere, which is expected since the flame has not yet reached the walls. Once the flame-wall interaction occurs, the flame adopts the so-called finger shape due to flame stretching in the direction of motion along the x-axis. The hemi-sphere to finger shape transition was not captured with the two-directional schlieren visualization since the first set of images were collected 50 mm from the ignition point. However, a highly symmetric flame is present during the finger-shape

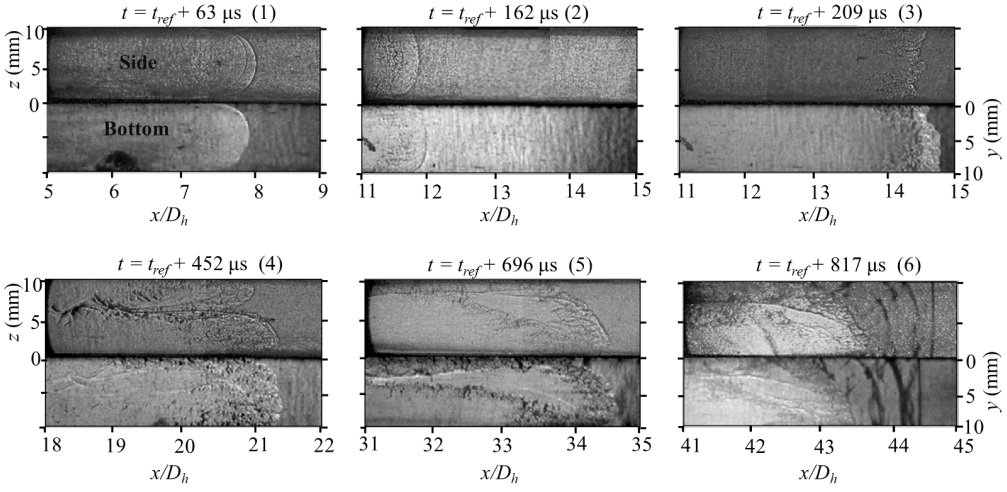

(a)

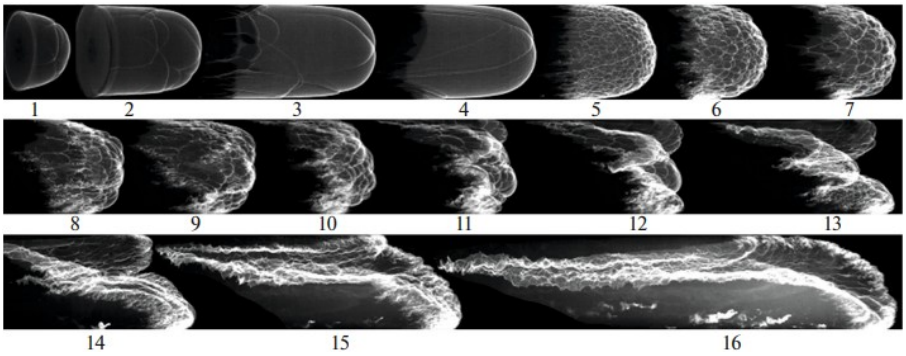

(b)

Figure 1: (a) Two-directional schlieren visualization of the CH_4-O_2 FA in a squared channel. (b) Measurement of spontaneous chemiluminescence of CH* for the C_2H_2-O_2-Ar FA in a cylindrical channel (Krivosheyev et al. [4])

stage, which corresponds to a region of relatively low velocity. Figure 2 presents the profile of (a) time (t) and (b) axial-velocity (u) along the tube, both normalized using fundamental combustion properties of the mixtures. From the results in [4], the evolution dynamics from the hemi-spherical to finger-shape flame exhibits a constant increase of the flame velocity due to the the flame surface area increase.

After the finger-shaped flame, at $t = t_{ref} + 162$ μs, the flame velocity plateaus, accompanied by flame surface instabilities but with an overall symmetrical morphology. The same behavior was captured by [4] in the images $5 - 7$. The appearance of this cellular structure is a consequence of the Darrieus–Landau instabilities due to the expansion of burned gases. During this transition, a decrease in the flame velocity is observed in both studies; see Figure 2 (b). At $t = t_{ref} + 209$ μs the flame morphoplogy is completely modified to a very irregular and asymmetrical shape, which can be confirmed with certainty thanks to the two-directional schlieren visualization. Both, the side- and bottom-view show flames that are similar to those presented in [4] in the images $10 - 12$. During this transition, as the flame propagates, the number of flame cells decrease but their size seems to increase and stretch in the flow direction.

At $t = t_{ref} + 452$ μs, two very different structures are observed in each view of the two-directional schlieren visualization. On the side view, there are two stretched flame fronts in the flow direction, having both different lengths and widths. This behavior is very similar to that shown in [4] in image 14.

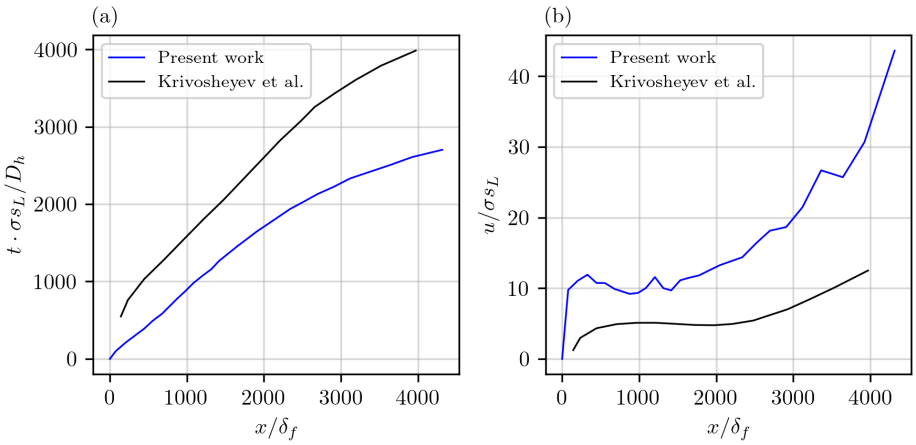

Figure 2: Non-dimensional (a) time, $t \cdot \sigma s_L/D_h$, and (b) axial velocity, $u/\sigma s_L$, profiles as a function of normalized axial position, x/δ_f. Symbols σ, s_L, and δ_f are the respective expansion ratio, laminar burning velocity and thermal flame thickness for each mixture; D_h is the hydraulic diameter.

However, in the bottom view, the flame takes a conical shape centered in the channel. Only a flame front can be observed. This behavior is not captured in any of the images presented in [4], providing further evidence of the relevance of the SSV. At $t = t_{ref} + 696$ μs the flame front takes a conical shape on both the side- and bottom-view but preferentially propagating along one side of the channel. This behavior is also reported in [4] in images $15 - 16$. Krivosheyev et al. [4] reported that the orientation of the flame front relative to the tube perimeter is probably random. At this stage of propagation, the flame starts to accelerate dramatically due to the increase of the surface area, as can be seen in Figure 2 (b) for both studies.

Finally, at $t = t_{ref} + 817$ μs, it is possible to observe a much faster conical flame (see Figure 2 (b)) which generates shock waves ahead of it as a result of the strong FA at this stage. Note that in [4], the shocks present in the preheated zone between the first precursor shock and the flame front cannot be resolved by direct observation (CH^* chemiluminescence). Note that the characterization of preheated zones is not possible in their setup without correcting for the *lensing effect* that arises when attempting to perform schlieren through thick curved transparent sections. However, with the SSV presented here, the shock waves that form in the preheated zone can be readily visualized. Subsequently, detonation onset occurs, which is out of the scope of the present study.

3.2 Discussion

To analyze the possible reasons for these similarities, the fundamental combustion properties of both mixtures (see Table 1) are computed. The properties listed are the laminar flame speed (s_L), the expansion ratio (σ), the Zel'dovich number (β), the laminar flame thickness (δ_t), the adiabatic flame temperature (T_b), and the D_h/δ_t ratio. The latter was calculated using Cantera. Dorofeev et al. [7] analyzed the behavior of turbulent flame propagation in obstructed channels for hydrogen mixtures using a large experimental database. They concluded that fundamental flame parameters can be used to estimate the potential for effective FA for a given mixture. Since these parameters depend mainly on the thermodynamic properties of the mixture, it is expected that the limits obtained in [7] change for the mixtures CH_4/O_2 and $C_2H_2/O_2/Ar$. However, in this work, the limits in [7] will be considered as a base, since no similar works were found for hydrocarbons. The authors showed that scale plays an important role during the FA process since the rate of flame acceleration and the propagation speed of slow flames tend to

increase with the scale in most cases. However, at sufficiently large scales ($D_h/\delta_t > 100$) it was found that FA's propensity seems to be only a function of the mixture composition. As shown in Table 1, both mixtures have ratios $D_h/\delta_t > 100$. Namely, 112.1 and 201.7 for mixture 1 and 2, respectively. Note that δ_t for mixture 2 is 3.3 times larger than that for mixture 1; however, the bigger scale of the channel used in [4] compensates for this effect and results in a higher D_h/δ_t ratio. Based on the results obtained in [7], the high D_h/δ_t ratios for both mixtures may explain the similarities observed as in spite of the difference in scale, the FA dynamics is similar for the tests considered. Note that previous work (in [7] and references therein) has drawn these conclusions based on computed velocities from flame position data alone. To our knowledge, however, side-by-side comparisons of the flame morphologies during the entire FA process at different scales had not been carried out until now.

Table 1: Combustion properties of the mixtures of interest at $T_0 = 300$ K.

Mixture	**Composition**	p_0 [kPa]	s_L [m/s]	σ	β	δ_t [mm]	T_b [K]	D_h/δ_t
1	CH_4 + $2O_2$	100	3.162	12.645	4.3	0.0892	3051.8	112.1
2	C_2H_2 + $2.5O_2$ + 1.17Ar	16	5.781	12.022	3.6	0.2975	3004.4	201.7

Another important conclusion from the work of Dorofeev et al. [7] was that the potential for effective FA is defined mainly by the value of the mixture expansion ratio, σ. The authors found that the development of fast combustion regimes is only possible for mixtures with $\sigma > 3.75$ for H_2-air mixtures; the cases discussed here with low-size hydrocarbons exhibit σ values significantly larger. Note that the difference in σ for both mixtures is only $5\,\%$ and given that $D_h/\delta_t > 100$, it seems that σ alone governs the flame morphologies during the FA process; additional tests should be performed for different mixtures with similar σ to verify this conclusion. Lastly, note that the Zel'dovich numbers, β, are 4.3 and 3.6 for mixture 1 and 2, respectively; also quite close. According to [7], β indicates the ability of turbulent mixing to quench the combustion process, influencing the behavior of the flame stretch and curvature by turbulent motions, and thus the flame morphology. This similarity is influenced by the fact of having very similar T_b, as shown in Table 1, since β depends on this variable according to the expression $\beta = E_a/(R_u T_b)(T_b - T_0)/T_b$, where T_0 is the initial temperature of the mixture and E_a is the activation energy, which has the values of 121.2 kJ/mol and 99.6 kJ/mol for mixture 1 and 2, respectively. Comparison of the results shown in Figure 2 with the raw $x - t$ and $u - x$ data (not presented due to space limitations) shows that normalization with the scaling proposed, based on fundamental combustion properties, results in lines with comparable slopes throughout the FA process; note that the vertical shift may stem from the difference in scale though the use of D_h should have in principle accounted for it. The trends shown seem to be related to the similar flame morphologies discussed in subsubsection 3.1 and suggest that under the conditions considered, most of the FA process scales with with laminar flame properties.

4 Conclusions

The flame morphologies developed during FA for stoichiometric CH_4-O_2 mixture were captured using SSV in a 1-m long fully optically accessible channel of square cross section (10×10 mm^2). The results are compared with those obtained by Krivosheyev et al. [4] via direct observation of CH^* chemiluminescence in a cylindrical tube of 60 cm in diameter and 6 m in length for a C_2H_2-O_2-Ar mixture. The main learnings of this work are as follows:

- Different morphologies were obtained during the FA process: (i) a finger-shaped flame, which is a consequence of the flame/wall interaction. (ii) a symmetrical flatter and corrugated flame that

forms due to the gas-dynamic effects (i.e., Darrieus-Landau); the flame accelerates as a result of the increase in flame surface area. (iii) an asymmetric flame with fewer but larger cells. (iv) a very irregularly shaped flame front that transitions to a more regular conical shape; this morphology remains unchanged until DO.

- Similar morphologies were observed by Krivosheyev et al. [4] although the flame front accelerates at a slower rate for the case with the $C_2H_2/O_2/Ar$ mixture. These similarities are interesting since the tests were performed under different conditions, i.e., different hydrocarbon fuel, channel geometry and scale.

- The similar morphologies presented seem to be due to the high D_h to δ_t ratio and the similar values of σ and β for the mixtures evaluated. The former indicates that scale does not seem to play an important role in the FA process, being mainly mixture dependent at these conditions, whereas the latter suggests that the flame morphology depends mainly on thermodynamic (σ) and kinetic (β) properties of the reactive mixture that can be computed *a priori*. This hypothesis should be verified further.

Acknowledgements

The authors gratefully acknowledge the financial support from *l'Agence Nationale de la Recherche* Program JCJC (FASTD ANR-20-CE05-0011-01) and FM Global.

References

[1] Dandan Liu, Zhaorong Liu, and Huahua Xiao. Flame acceleration and deflagration-to-detonation transition in narrow channels filled with stoichiometric hydrogen-air mixture. *International Journal of Hydrogen Energy*, 47(20):11052–11067, 2022.

[2] Mohammad Hosein Shamsadin Saeid, Javad Khadem, and Sobhan Emami. Numerical investigation of the mechanism behind the deflagration to detonation transition in homogeneous and inhomogeneous mixtures of h2-air in an obstructed channel. *International Journal of Hydrogen Energy*, 46(41):21657–21671, 2021.

[3] Yves Ballossier. *Topologies de l'accélération de flammes d'H2-O2-N2 dans des canaux étroits: de l'allumage jusqu'à la détonation*. PhD thesis, Ecole nationale supérieure de mécanique et d'aérotechnique, 2021.

[4] PN Krivosheyev, AO Novitski, and OG Penyazkov. Evolution of the reaction front shape and structure on flame acceleration and deflagration-to-detonation transition. *Russian Journal of Physical Chemistry B*, 16(4):661–669, 2022.

[5] Yves Ballossier, Florent Virot, and Josué Melguizo-Gavilanes. Strange wave formation and detonation onset in narrow channels. *Journal of Loss Prevention in the Process Industries*, 72:104535, 2021.

[6] Yves Ballossier, Florent Virot, and J Melguizo-Gavilanes. Flame propagation and acceleration in narrow channels: sensitivity to facility specific parameters. *Shock Waves*, 31(4):307–321, 2021.

[7] SB Dorofeev, MS Kuznetsov, VI Alekseev, AA Efimenko, and W Breitung. Evaluation of limits for effective flame acceleration in hydrogen mixtures. *Journal of loss prevention in the process industries*, 14(6):583–589, 2001.